Materials Science and Engineering A 528 (2011) 4807–4811

Contents lists available at ScienceDirect

Materials Science and Engineering A

journal homepage: www.elsevier.com/locate/msea

Strain softening in nanocrystalline Ni–Fe alloy induced by large HPT revolutions

S. Ni[a], Y.B. Wang[a], X.Z. Liao[a,*], R.B. Figueiredo[b], H.Q. Li[c], Y.H. Zhao[d], E.J. Lavernia[d], S.P. Ringer[e], T.G. Langdon[f,g], Y.T. Zhu[h]

[a] School of Aerospace, Mechanical and Mechatronic Engineering, The University of Sydney, Sydney, NSW 2006, Australia
[b] Department of Metallurgical and Materials Engineering, Federal University of Minas Gerais, Belo Horizonte, MG 31270-901, Brazil
[c] Los Alamos National Laboratory, Los Alamos, NM 87545, USA
[d] Department of Chemical Engineering and Materials Science, University of California, Davis, CA 95616, USA
[e] Australian Centre for Microscopy & Microanalysis, The University of Sydney, NSW 2006, Australia
[f] Departments of Aerospace & Mechanical Engineering and Materials Science, University of Southern California, Los Angeles, CA 90089-1453, USA
[g] Materials Research Group, School of Engineering Sciences, University of Southampton, Southampton SO17 1BJ, UK
[h] Department of Materials Science & Engineering, North Carolina State University, Raleigh, NC 27659-7919, USA

ARTICLE INFO

Article history:
Received 31 January 2011
Received in revised form 28 February 2011
Accepted 1 March 2011

Keywords:
Severe plastic deformation
Nanocrystalline materials
Strain softening
Dislocation density
Lomer–Cottrell locks

ABSTRACT

The influence of strain on the hardness of an electrochemically deposited nanocrystalline Ni–20 wt.% Fe alloy processed by high-pressure torsion (HPT) for 20 and 30 revolutions was investigated. Strain softening followed by a stable hardness value was observed. Structural investigations revealed that, while dislocation density was important, continuous grain growth played a major role in the strain softening. The stable hardness indicates that an equilibrium structure was achieved, supporting a dynamic balance between deformation-induced grain growth and grain refinement and between deformation-induced dislocation generation and dislocation annihilation.

1. Introduction

Severe plastic deformation (SPD) techniques, including equal channel angular pressing and high-pressure torsion (HPT), have been widely used to produce bulk ultrafine-grained (UFG, <1 μm) and nanocrystalline (nc, <100 nm) materials for superior mechanical properties [1–4]. Extensive investigations were carried out to understand the deformation mechanisms at different stages of the grain refinement process. It is well established that deformation induced grain refinement occurs via dislocation activities and/or the formation of twins, as well as via the interaction between dislocations and twin boundaries [5–10]. There is always a minimum average grain size in a deformation-induced grain refinement process for any specific material and under any specific deformation condition [11]. This minimum average grain size is determined by both intrinsic material properties, such as stacking fault energy, and by extrinsic processing parameters [11,12]. One of the factors leading to a minimum grain size is deformation-induced grain growth. The minimum grain size is achieved by the dynamic balance between grain refinement and grain growth processes. Coarse-grained materials were used to investigate deformation-induced grain refinement processes in which the grain growth processes are overwhelmed by the much stronger effect of grain refinement [5–12]. By contrast, deformation-induced grain growth has been readily observed in materials where the starting grain sizes were much smaller than the minimum grain sizes achievable by deformation-induced grain refinement [13–21].

A deformation-induced grain growth process is usually accompanied by an evolution in the dislocation density [15,22–24]. Previous investigations reported a complicated dislocation density evolution during HPT-induced grain growth in nc Ni–Fe alloys. Specifically, the dislocation density increased in the very early stages of HPT processing because of the large number of dislocations emitted from grain boundaries [24,25]. The high density of dislocations in nc grains was very unstable and further deformation reduced the dislocation density [22,24]. As grain growth continued, a high density of Lomer–Cottrell (L–C) locks was formed, leading to a subsequent increase in the dislocation density [22,24]. The L–C lock formation was predicted for deformed nc metals on the basis

* Corresponding author. Tel.: +61 2 9351 2348; fax: +61 2 9351 7060.
E-mail address: xiaozhou.liao@sydney.edu.au (X.Z. Liao).

0921-5093/$ – see front matter © 2011 Elsevier B.V. All rights reserved.
doi:10.1016/j.msea.2011.03.007

of Molecular Dynamic simulations in nc Al [25] and it has been experimentally verified in various nc materials [24,26,27].

The evolution of dislocation density during a deformation-induced grain growth process significantly affects the mechanical behavior of materials. In related work, Li et al. [15,23] reported that plastic deformation via cold rolling of a nc Ni–Fe alloy resulted in a reduction of dislocation density and this produced strain softening. The HPT processing of a nc Ni–20 wt.% Fe alloy to different strain values showed that (1) strain hardening, strain softening and a second strain hardening occurred consecutively; (2) the hardness evolution followed the dislocation density evolution; (3) the effect of grain growth on hardness evolution was not as strong as that of the dislocation density evolution; and (4) the upper grain size limit of grain growth was not achieved for HPT under 6 GPa for up to 10 revolutions [24,28].

It is therefore of interest to provide insight into the following questions. First, how does the structure, including grain size and dislocation density, of the nc Ni–20 wt.% Fe alloy continue to evolve with further increases in HPT strain? Second, how does the structural evolution further affect the hardness of the material? Third, will an equilibrium structure be achieved and, if so, will the final average grain size be comparable to that obtained via HPT-induced grain refinement? To answer these questions, HPT processing of the alloy was conducted through 20 and 30 revolutions, detailed hardness testing was performed, and the structural evolution was characterized using X-ray diffraction (XRD) and transmission electron microscopy (TEM). The results reveal the presence of a strain softening stage followed by a stable hardness stage. The strain softening is due to continuous grain growth and a reduction in the dislocation density while the stable hardness stage indicates that an equilibrium structure was achieved.

2. Experimental material and procedures

An electrochemically deposited nc Ni–20 wt.% Fe alloy was purchased from the Integran Technologies Inc (Pittsburgh, USA) after synthesizing using the method described in Ref. [29]. The as-deposited material was a non-equilibrium supersaturated solid solution with a single phase face-centred cubic structure [29]. Disks with a diameter slightly less than 10 mm and a thickness of ~1.5 mm were polished on both sides using sand papers (400–2000 grade) until their thickness reached 0.8 mm. These disks were then subjected to HPT processing under an applied pressure of 6 GPa and a rotation rate of 1 rpm for 20 and 30 revolutions, respectively, using a quasi-constrained HPT facility [30]. Tracking of the temperature rise during the HPT process indicated a rapid rise from ~25 °C to ~50 °C after 5 turns and then a slow increase to ~70 °C after 30 turns.

After HPT processing, the disks were mechanically polished to produce a mirror-like surface using diamond lapping films (30–1 μm) for hardness testing. The hardness test was conducted using a Leco LV700AT hardness tester equipped with a Vickers indenter and with a load of 10 kg applied at each point for 15 s and at different radial positions of each disk. A schematic diagram was presented earlier [28] showing the positions for the hardness measurements on each disk. The error bar for each mean hardness value was obtained from the tested highest hardness value to the lowest value.

The XRD measurements were performed using a Siemens D5000 X-ray diffractometer on the central part ($r < 2.5$ mm) and the edge part ($2.5\text{ mm} < r < 5\text{ mm}$) of each disk. The XRD peak broadening was used to evaluate the dislocation density [24]. The errors in these dislocation density measurements were assessed by scanning each specimen three times and they were demonstrated to be less than 6% which is significantly smaller than the dislocation density changes between different deformation stages. TEM samples were prepared via standard techniques [28] and experiments were performed using a JEOL JEM-3000F operating at 300 kV. The average grain sizes were statistically estimated by measuring at least 200 grains with clear grain boundaries in bright-field TEM images where the grains exhibited strong diffraction conditions and therefore appeared dark.

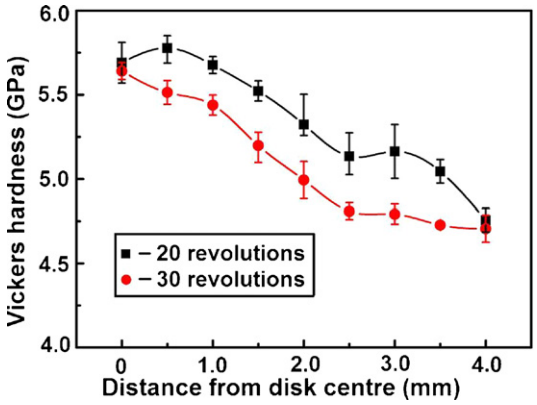

Fig. 1. Vickers hardness plotted against distance from the centres of disks after HPT processing for 20 and 30 revolutions.

3. Experimental results

3.1. The evolution of hardness

Fig. 1 shows Vickers hardness values at different radial positions on the 20- and 30-revolution HPT disks. The Vickers hardness for the 20-revolution HPT disk decreased from the radius of ~1.0 mm towards the edge of the disk, reaching the lowest value of ~4.75 GPa at the radial position of 4.0 mm. The Vickers hardness for the 30-revolution HPT disk also experienced a sharp decrease from the disk centre to the radius of 2.5 mm and then levelled off to a lowest value of ~4.75 GPa.

In order to better understand the effect of HPT-induced plastic deformation on the hardness evolution, the hardness values are plotted as a function of the von Mises equivalent strain, ε, in Fig. 2. The equivalent strain is defined as $\varepsilon = 2\pi Nr/h\sqrt{3}$, where r is the distance from the disk centre, h is the thickness of the disk and N is the number of HPT revolutions [31]. For comparison, previously published data for HPT revolutions up to 10 [28] are re-plotted in Fig. 2(a) together with the data for 20 and 30 revolutions shown in Fig. 2(b). The hardness values at equivalent strains smaller than 180 in Fig. 2(b) are in agreement with those shown in Fig. 2(a) although, as discussed previously [28], the strain softening stage with strain values from 20 to 35 in disks with low numbers of HPT revolutions was not observed at larger numbers of revolutions. Beyond a strain value of 180, the hardness decreases gradually until reaching a lowest value of ~4.7 GPa at a strain value of ~340. Further deformation had no additional effect on the hardness. Following the designations given earlier [28], the strain softening stage and the subsequent level hardness stage are denoted deformation stages V and VI, respectively. Thus, stage V corresponds to a region with radius from 1.5 to 4 mm of the 20-revolution disk and the central part ($r < 2.5$ mm) of the 30-revolution disk, whereas stage VI corresponds to the edge part ($r > 2.5$ mm) of the 30-revolution disk.

3.2. The evolution of grain size and dislocation density

Fig. 3 shows typical low magnification TEM images of samples at (a) deformation stage V and (b) deformation stage VI, respec-

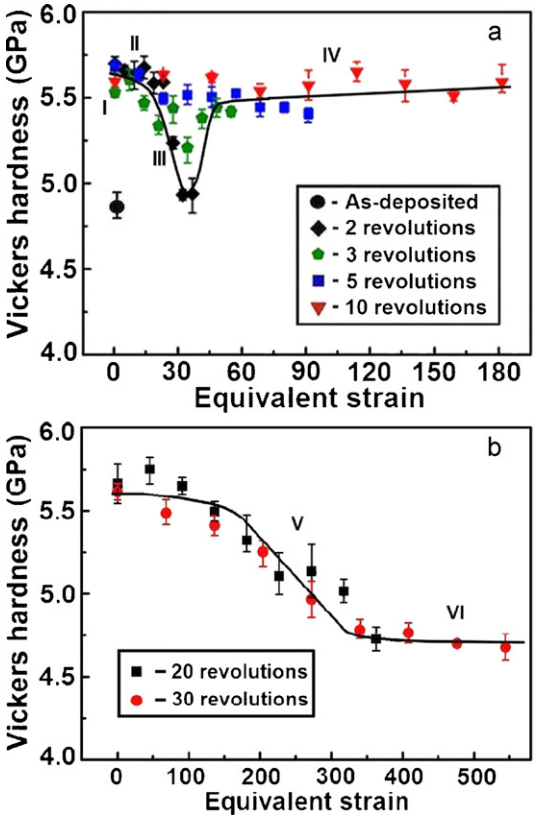

Fig. 2. Vickers hardness plotted against von Mises equivalent strain for disks with HPT processing for 2, 3, 5, and 10 revolutions [28] (a), and for 20 and 30 revolutions (b).

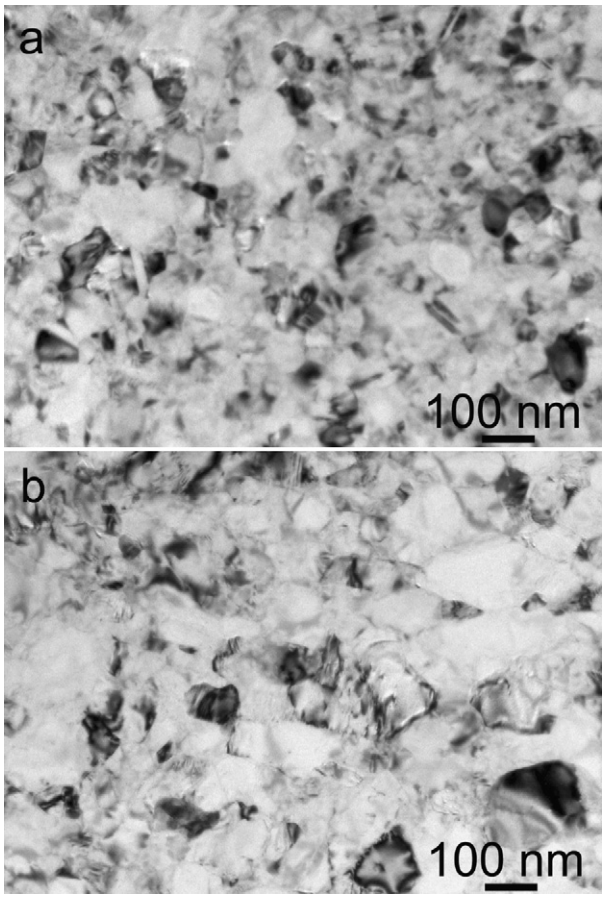

Fig. 3. Typical low magnification TEM images of the edge of a 20-revolution HPT disk (a) and the edge of a 30-revolution HPT disk (b).

tively. The average grain sizes were estimated as ~72 nm in stage V and ~120 nm in stage VI. TEM observations demonstrated that the grain size distributions throughout deformation stage VI remained roughly constant. The average dislocation density calculated from XRD data was estimated as $\sim 2.1 \times 10^{15}\ m^{-2}$ and $\sim 2.0 \times 10^{15}\ m^{-2}$ at the edge parts of the 20- and 30-revolution HPT disks corresponding to the late stage V and stage VI, respectively. The dislocation density at the central part of the 20-revolution disk was $\sim 2.6 \times 10^{15}\ m^{-2}$. Because the central part of the 20-revolution disk includes a small amount of material in deformation stage IV and because the dislocation density in stage IV is $\sim 6.0 \times 10^{15}\ m^{-2}$, it is clear that the dislocation density drops significantly during the transition from deformation stage IV to stage V and, in addition, there is litle change in the dislocation density in deformation stages V and VI. Combined with the earlier data [28], Table 1 lists the average grain sizes and dislocation densities of the material before HPT and in all 6 HPT deformation stages. This tabulation reveals a continuous grain growth as the strain increases and an obvious dislocation density reduction from stage IV to V. The average dislocation density reached an equilibrium value in the late stage V and stage VI.

Table 1
Dislocation densities calculated by XRD data and average grain sizes measured from TEM images of disks at different deformation stages. The ranges of equivalent strain at different deformation stages are also listed.

Deformation stage	Equivalent strain	Dislocation density (m^{-2})	Average grain size (nm)
As-deposited	0	2.2×10^{15}	21
I	0–4.5	3.6×10^{15}	22
II	4.5–20	5.8×10^{15}	30
III	20–35	4.1×10^{15}	35
IV	35–182	6.0×10^{15}	50
V	180–340	2.1×10^{15}	72
VI	340–550	2.0×10^{15}	120

As reported previously, high densities of L–C locks were formed in deformation stage IV which is a direct consequence of the deformation-induced grain growth via grain rotation and is responsible for a significant increase in dislocation density and for strain hardening [24,28]. As deformation proceeds to stages V and VI, the dislocation density decreased dramatically from $\sim 6.0 \times 10^{15}\ m^{-2}$ in deformation stage IV [24] to $\sim 2.0 \times 10^{15}\ m^{-2}$. Careful high-resolution TEM observations revealed that the extent of L–C locking was significantly reduced in deformation stages V and VI, and the dislocation distributions and dislocation densities were similar in the two stages. Fig. 4 presents a high-resolution TEM image of a typical grain in deformation stage VI. As shown in Fig. 4(a), a contrast variation is seen within different regions of the grain, for example, region A and region B, as indicated by two white rectangles. The Fourier transformation of a large area covering both regions A and B, shown on the upper right corner of Fig. 4(a), confirms that regions A and B are part of a single grain. Fig 4(b) and (c) show enlarged high-resolution TEM images of areas A and B in Fig. 4(a), respectively. Fig. 4(b) shows that no defects exist in the grey areas in Fig. 4(a). From Fig. 4(c), no obvious misorientation was observed between the dark region and the grey region. Fig. 4(d) shows the Fourier-filtered image of a selected rectangular area in Fig. 4(c) in which dislocations were observed and marked with "T". Most of these dislocations are distributed randomly with only a few forming L–C locks. Detailed TEM analysis of the whole grain revealed that most of the large grain is dislocation-free while high densities of dislocations were distributed randomly but visible only within

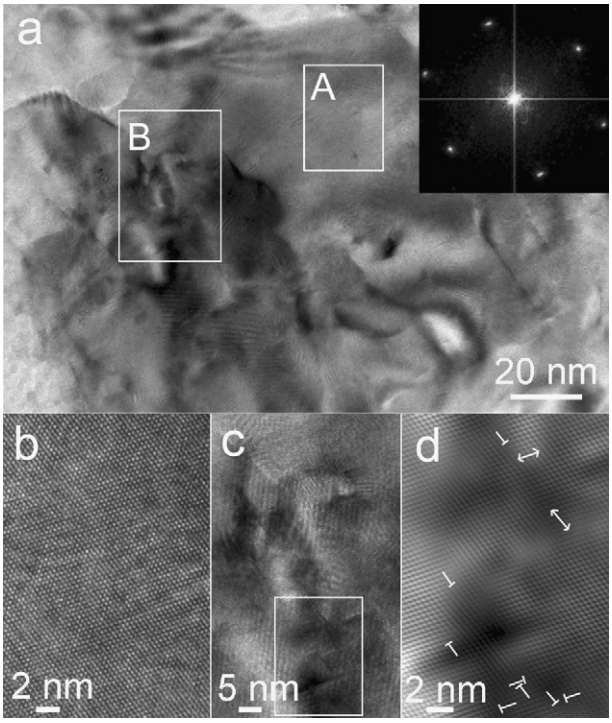

Fig. 4. (a) A high-resolution TEM image and its Fourier transformation of a grain at deformation stage VI. Selected rectangular areas marked with A and B in (a) are enlarged in (b) and (c), respectively. (d) A Fourier-filtered image of the selected rectangular area in (c).

limited areas which appeared dark because of the strain caused by the high densities of dislocations. The numbers of closely paired dislocations forming L–C locks in deformation stage IV decreased dramatically, indicating that the previously formed L–C locks were unlocked as deformation proceeded to higher strain values and they may have glided away and disappeared at grain boundaries.

4. Discussion

It is reasonable to anticipate that HPT-induced grain refinement and grain growth will lead to the same final grain sizes for materials with the same compositions and processed under the same external conditions. This is the case for HPT-induced grain refinement [32–34] and grain growth [13] of pure Ni, which reached equilibrium average grain sizes of ~105–170 nm and ~129 nm, respectively. This final average grain size is determined by extrinsic processing parameters and intrinsic material properties including the stacking fault energy, bulk modulus, melting temperature, and activation energy [11,12]. The maximum average grain size of ~120 nm achieved at the edge of the 30-revolution HPT Ni–Fe disks appears to represent the maximum grain size achievable by HPT-induced grain growth as there is no observable average grain size change in stage VI. It is reasonable to anticipate that the measured temperature rise to ~70 °C during HPT processing will have only a minor effect on the HPT-induced grain growth.

It has been reported that HPT-induced grain growth occurs via grain rotation when the original grain sizes are ~20 nm [14,24]. This mechanism leads to the formation of large fractions of low-angle sub-grain boundaries in the early stages of HPT processing. Because it is difficult to identify low-angle grain boundaries in the 20- and 30-revolution HPT disks, the grain growth in the later stages of HPT processing in this study should occur via the mechanism of grain boundary migration in which large grains grow at the expense of smaller grains [35].

The formation and dissociation of L–C locks were observed in deformation stage IV and the transition point of stage IV to stage V, respectively. Both the formation and the dissociation of L–C locks have been predicted by molecular dynamic simulations [36–39]. The formation of L–C locks occurs in nc materials when two dislocations on different glide planes approach each other [24,26] or when a dislocation interacts with a twin boundary [40,41]. The formation followed by dissociation of L–C locks was observed in a nc Pt ultrathin film by in situ deformation TEM [27]. When two full dislocations meet under an applied stress on two intersecting slip planes, they react to reach a low energy configuration and thereby form a stable junction such as an L–C lock [42]. The structure of an L–C lock consists of a junction segment along the line of intersection between the glide planes of the two initial full dislocations and four arms of the junction which are dissociated in their glide planes [38]. With increasing stress, the length of the junction segment decreases via an "unzipping" mechanism, which takes place as the two dislocations forming the junction segment are pulled apart under the action of the applied stress so that the junction breaks [38]. The present TEM observations indicate that the L–C locks formed in the early stages of the HPT deformation process can unlock in the later stages of HPT when an external force is available to activate the L–C lock dissociation.

This study reveals a strain softening stage and a stable hardness stage following the previous four deformation stages reported earlier [28]. While the hardness evolution in deformation stages I–IV was determined mainly by the evolution of the dislocation density [28], the hardness evolution in deformation stages V and VI follows a different mechanism. As indicated from the experimental results, the dislocation density remained approximately constant in stage V and VI after a sharp drop during the transition from deformation stage IV to stage V. However, the grain size increased continuously before reaching a stable size in stage VI, indicating that the grain size evolution is a dominant factor that determines the hardness evolution in stage V. Molecular dynamic simulations [43] have confirmed that the Hall–Petch relationship operates for materials having grain sizes similar to those visible in deformation stage V so that an increasing grain size reduces the hardness. This is consistent with the present observations in deformation stage V.

The stable hardness stage is associated both with an average grain size at or close to the stable grain size of an HPT-induced grain growth process and with a constant dislocation density. It is therefore proposed that the stable and equilibrium hardness value achieved in this stage is the result of balances between deformation-induced grain growth and grain refinement and between deformation-induced dislocation generation and dislocation annihilation.

5. Conclusions

An electrochemically deposited nanocrystalline Ni–20 wt.% Fe alloy was processed by high-pressure torsion to 20 and 30 revolutions. A strain softening stage and a stable hardness stage were observed. Grain growth occurred continuously, reaching a maximum average grain size of ~120 nm at the edge of the 30-revolution HPT disks. The strain softening stage is attributed to the dominant role of grain growth and a reduction in the dislocation density. The latter is due to the dissociation of Lomer–Cottrell locks formed in the early stages of HPT deformation. The stable hardness stage results from balances between deformation-induced grain growth and grain refinement and between dislocation generation and dislocation annihilation.

Acknowledgements

The authors are grateful for scientific and technical input and support from the Australian Microscopy & Microanalysis Research Facility node at the University of Sydney. This project is supported by the Australian Research Council [Grant No. DP0772880 (S.N., Y.B.W., and X.Z.L.)], the LDRD program of Los Alamos National Laboratory (H.Q.L.), the Office of Naval Research [Grant No. N00014-08-1-0405 (Y.H.Z. and E.J.L.)], the National Science Foundation of the United States (Grant No. DMR-0855009, T.G.L.) and the U.S. Army Research Office and Army Research Laboratory (Y.T.Z.). S.N. also appreciates support from the China Scholarship Council.

References

[1] S.X. McFadden, R.S. Mishra, R.Z. Valiev, A.P. Zhilyaev, A.K. Mukherjee, Nature (London) 398 (1999) 684–686.
[2] R.Z. Valiev, I.V. Alexandrov, Y.T. Zhu, T.C. Lowe, J. Mater. Res. 18 (2002) 5–8.
[3] D. Jia, Y.M. Wang, K.T. Ramesh, E. Ma, Y.T. Zhu, R.Z. Valiev, Appl. Phys. Lett. 79 (2001) 611–613.
[4] P.P.V. Liddicoat, X.Z. Liao, Y.H. Zhao, Y.T. Zhu, M.Y. Murashkin, E.J. Lavernia, R.Z. Valiev, S.P. Ringer, Nature Commun. 1 (2010) 63.
[5] N. Hansen, X. Huang, Acta Mater. 46 (1998) 1827–1836.
[6] X.Z. Liao, Y.H. Zhao, Y.T. Zhu, R.Z. Valiev, D.V. Gunderov, J. Appl. Phys. 96 (2004) 636–640.
[7] F. Dalla Torre, R. Lapovok, J. Sandlin, P.F. Thomson, C.H.J. Davies, E.V. Pereloma, Acta Mater. 52 (2004) 4819–4832.
[8] Y.S. Li, N.R. Tao, K. Lu, Acta Mater. 56 (2008) 230–241.
[9] J.W. Christian, S. Mahajan, Prog. Mater. Sci. 39 (1995) 1–157.
[10] Y.B. Wang, X.Z. Liao, Y.H. Zhao, E.J. Lavernia, S.P. Ringer, Z. Horita, T.G. Langdon, Y.T. Zhu, Mater. Sci. Eng. A 527 (2010) 4959–4966.
[11] F.A. Mohamed, Acta Mater. 51 (2003) 4107–4119.
[12] A.P. Zhilyaev, G.V. Nurislamova, B.K. Kim, M.D. Baró, J.A. Szpunar, T.G. Langdon, Acta Mater. 51 (2003) 753–765.
[13] X.Z. Liao, A.R. Kilmametov, R.Z. Valiev, H.S. Gao, X.D. Li, A.K. Mukherjee, J.F. Bingert, Y.T. Zhu, Appl. Phys. Lett. 88 (2006) 021909.
[14] Y.B. Wang, J.C. Ho, X.Z. Liao, H.Q. Li, S.P. Ringer, Y.T. Zhu, Appl. Phys. Lett. 94 (2009) 011908.
[15] L. Li, T. Ungár, Y.D. Wang, G.J. Fan, Y.L. Yang, N. Jia, Y. Ren, G. Tichy, J. Lendvai, H. Choo, P.K. Liaw, Scripta Mater. 60 (2009) 317–320.
[16] G.J. Fan, L.F. Fu, H. Choo, P.K. Liaw, N.D. Browning, Acta Mater. 54 (2006) 4781–4792.
[17] A.P. Zhilyaev, A.A. Gimazov, E.P. Soshnikova, Á. Révész, T.G. Langdon, Mater. Sci. Eng. A 489 (2008) 207–212.
[18] G.J. Fan, Y.D. Wang, L.F. Fu, H. Choo, P.K. Liaw, Y. Ren, N.D. Browning, Appl. Phys. Lett. 88 (2006) 171914.
[19] S. Cheng, Y.H. Zhao, Y.M. Wang, Y. Li, X.L. Wang, P.K. Liaw, E.J. Lavernia, Phys. Rev. Lett. 104 (2010) 255501.
[20] S. Cheng, Y.H. Zhao, Y.Z. Guo, Y. Li, Q.M. Wei, X.L. Wang, Y. Ren, P.K. Liaw, H. Choo, E.J. Lavernia, Adv. Mater. 21 (2009) 5001–5004.
[21] H.M. Wen, Y.H. Zhao, Y. Li, O. Ertorer, R.Z. Valiev, E.J. Lavernia, Phil. Mag. 90 (2010) 4541–4550.
[22] Y.B. Wang, J.C. Ho, Y. Cao, X.Z. Liao, H.Q. Li, Y.H. Zhao, E.J. Lavernia, S.P. Ringer, Y.T. Zhu, Appl. Phys. Lett. 94 (2009) 091911.
[23] L. Li, T. Ungár, Y.D. Wang, J.R. Morris, G. Tichy, J. Lendvai, Y.L. Yang, Y. Ren, H. Choo, P.K. Liaw, Acta Mater. 57 (2009) 4988–5000.
[24] S. Ni, Y.B. Wang, X.Z. Liao, S.N. Alhajeri, H.Q. Li, Y.H. Zhao, E.J. Lavernia, S.P. Ringer, T.G. Langdon, Y.T. Zhu, Scripta Mater. 64 (2011) 327–330.
[25] V. Yamakov, D. Wolf, S.E. Phillpot, A.K. Mukherjee, H. Gleiter, Nature Mater. 1 (2002) 45–48.
[26] X.L. Wu, Y.T. Zhu, Y.G. Wei, Q. Wei, Phys. Rev. Lett. 103 (2009) 205504.
[27] L.H. Wang, X.D. Han, P. Liu, Y.H. Yue, Z. Zhang, E. Ma, Phys. Rev. Lett. 105 (2010) 135501.
[28] S. Ni, Y.B. Wang, X.Z. Liao, S.N. Alhajeri, H.Q. Li, Y.H. Zhao, E.J. Lavernia, S.P. Ringer, T.G. Langdon, Y.T. Zhu, Mater. Sci. Eng. A 528 (2011) 3398–3403.
[29] H.Q. Li, F. Ebrahimi, Mater. Sci. Eng. A 347 (2003) 93–101.
[30] A.P. Zhilyaev, T.G. Langdon, Prog. Mater. Sci. 53 (2008) 893–979.
[31] R.Z. Valiev, YuV. Ivanisenko, E.F. Rauch, B. Baudelet, Acta Mater. 44 (1996) 4705–4712.
[32] F. Dalla Torre, P. Spätig, R. Schaublin, M. Victoria, Acta Mater. 53 (2005) 2337–2349.
[33] N. Krasilnikov, W. Lojkowski, Z. Pakiela, R.Z. Valiev, Mater. Sci. Eng. A 397 (2005) 330–337.
[34] A.P. Zhilyaev, S. Lee, G.V. Nurislamova, R.Z. Valiev, T.G. Langdon, Scripta Mater. 44 (2001) 2753–2758.
[35] M. Legros, D.S. Gianola, K.J. Hemker, Acta Mater. 56 (2008) 3380–3393.
[36] M.J. Buehler, A. Hartmajer, M.A. Duchaineau, F.F. Abraham, H.J. Gao, Acta Mech. Sinica 21 (2005) 103–111.
[37] V.V. Bulatov, F.F. Abraham, L.P. Kubin, B. Devincre, S. Yip, Nature (London) 391 (1998) 669–672.
[38] D. Rodney, R. Phillips, Phys. Rev. Lett. 82 (1999) 1704–1707.
[39] V.B. Shenoy, R.V. Kukta, R. Phillips, Phys. Rev. Lett. 84 (2000) 1491–1494.
[40] Y.T. Zhu, J. Narayan, J.P. Hirth, S. Mahajan, X.L. Wu, X.Z. Liao, Acta Mater. 57 (2009) 3763–3770.
[41] Y.T. Zhu, X.L. Wu, X.Z. Liao, J. Narayan, L.J. Kecskés, S.N. Mathaudhu, Acta Mater. 59 (2011) 812–821.
[42] R. Madec, B. Devincre, L. Kubin, T. Hoc, D. Rodney, Science 301 (2003) 1879–1893.
[43] J. Schiøtz, K.W. Jacobsen, Science 301 (2003) 1357–1359.